Northumbria Research Link

Citation: Beatini, Valentina, Royer-Carfagni, Gianni and Tasora, Alessandro (2017) A regularized non-smooth contact dynamics approach for architectural masonry structures. Computers & Structures, 187. pp. 88-100. ISSN 0045-7949

Published by: Elsevier

URL: https://doi.org/10.1016/j.compstruc.2017.02.002 <https://doi.org/10.1016/j.compstruc.2017.02.002>

This version was downloaded from Northumbria Research Link: http://nrl.northumbria.ac.uk/38351/

Northumbria University has developed Northumbria Research Link (NRL) to enable users to access the University's research output. Copyright © and moral rights for items on NRL are retained by the individual author(s) and/or other copyright owners. Single copies of full items can be reproduced, displayed or performed, and given to third parties in any format or medium for personal research or study, educational, or not-for-profit purposes without prior permission or charge, provided the authors, title and full bibliographic details are given, as well as a hyperlink and/or URL to the original metadata page. The content must not be changed in any way. Full items must not be sold commercially in any format or medium without formal permission of the copyright holder. The full policy is available online: http://nrl.northumbria.ac.uk/policies.html

This document may differ from the final, published version of the research and has been made available online in accordance with publisher policies. To read and/or cite from the published version of the research, please visit the publisher's website (a subscription may be required.)

www.northumbria.ac.uk/nrl

northumbria UNIVERSITY NEWCASTLE

A regularized Non-Smooth Contact Dynamics approach for architectural masonry structures

Valentina BEATINI

Department of Architecture
Abdullah Gül University, Sumer Kampus, Kocasinan, 38280, Kayseri, Turkey. email: valentina.beatini@agu.edu.tr

Gianni ROYER-CARFAGNI

Department of Engineering
University of Parma, Parco Area delle Scienze 181/A, I 43100 Parma, Italy, email: gianni.royer@unipr.it
and
Construction Technologies Institute - Italian National Research Council (ITC-CNR)
Via Lombardia 49, I 20098 San Giuliano Milanese (Mi), Italy

Alessandro TASORA

Department of Engineering
University of Parma, Parco Area delle Scienze 181/A, I 43100 Parma, Italy, email: alessandro.tasora@unipr.it

Abstract

A Non-Smooth Contact Dynamic (NSCD) formulation is used to analyze complex assemblies of rigid blocks, representative of real masonry structures. A model of associative friction sliding is proposed, expressed through a Differential Variational Inequality (DVI) formulation, relying upon the theory of Measure Differential Inclusion (MDI). A regularization is used in order to select a unique solution and to avoid problems of indeterminacy in redundant contacts. This approach, complemented with an optimized collision detection algorithm for convex contacts, results to be reliable for dynamic analyses of masonry structures under static and dynamic loads. The approach is comprehensive, since we implement a custom NSCD simulator based on the Project Chrono C++ framework, and we design custom tools for pre- and post-processing through a user-friendly parametric design software. Representative examples confirm that the method can handle 3-D complex structures, as typically are architectural masonry constructions, under both static and dynamic loading.

Keywords: Non-Smooth Contact Dynamic (NSCD), Measure Differential Inclusion (MDI), associative friction, masonry, rigid blocks, dynamic analysis.

1 Introduction

An advanced rigid-body dynamics formulation is used to analyze assemblies of rigid blocks, representative of architectural masonry constructions, under static and dynamic loadings. The method is interfaced with design custom tools for pre-processing and post-processing through a user-friendly parametric design software, which allows the design of complex masonry structures in the three-dimensional space.

While the proposed model assumes blocks to be very stiff, it focuses on the reliable description of associative friction laws at the contact surfaces. This approach was introduced for masonry constructions by Kooharian [27], who envisioned the possibility of studying structures of this kind within the plasticity theory. Under the assumption of unilateral constraints and absence of tensile strength, limit analysis was used to calculate the load which causes instability at the contact surfaces between the blocks [23]. The reliability and advantages of this approach are founded on the characteristics of this type of structures, which are prone to instability failure because of the definite prevalence of compressive strength over tensile strength. Meanwhile, other analyses that require the exact knowledge of the material parameters are difficult to be applied, because masonry is a composite material for which the nature of the composing blocks and interlayers, as well as their interactions, is highly irregular and, therefore, uncertain. Experiments [6, 7] have provided evidence that, when a great number of blocks is organized into very complex arrangements, the stress percolation results to be highly localized, evidencing unloading islands in a stress stream.

Compared to the thrust-line graphical method [13, 10], still used in the current practice for preliminary analyses, the dynamical formulations of the problem, as indicated by Livesley and Gilbert [30, 21], provide significant advances because all the possible types of movements are considered and the interactions between all blocks can be fully appreciated. In particular, the method proposed here is set within the category of the Non-Smooth Contact Dynamic (NSCD) framework, firstly developed by Moreau [32] to handle specifically unilateral constraints. This provides a proper definition of contacts, whose value can be clarified comparing the NSCD approach with alternative mathematical formulations, namely the Ordinary Differential Equations (ODE) and the Differential Algebraic Equations (DAE) formulations [19], which have been more often applied to masonry. The DAE approach is the more refined and expresses constraint equations together with the differential equations, as it happens in the classical multi-body dynamics at the base of most Discrete Element Method software (DEM) [12]. In methods of this kind, contacts are modeled with penalty functions, which represent spring-damper elements whose flexibility

can be adjusted to match the real stiffness of the contact surfaces, for instance using the Hertz-Mindlin theory or similar models. However, a physically accurate compliance of contact points with high stiffness coefficients results in steep penalty functions, something that would require extremely short time steps in most ODE or DAE integrator algorithm, at the point of being very inefficient or even unusable [22].

More specifically, modeling very rigid blocks provides the opportunity to reproduce the stick-slip transition, representing a sudden change in motion at collision. This is a typical contact phenomenon that strongly affects the failure mechanism and the corresponding ultimate load. Our model, by leveraging on the theory of Measure Differential Inclusions (MDI) [34, 33], describes forces and accelerations as distributions of measures, while velocities are functions of Bounded Variation (BV), not necessarily continuous. Instead, the aforementioned alternative approaches describe velocities through smooth functions, which therefore cannot represent the sudden changes in motion at collision [1]. Despite workarounds have been proposed [35, 20], they actually detriment the clarity of the model and the initial advantage of those methods in terms of computational effort.

The NSCD framework implemented here has been developed by one of the authors within the Project Chrono, a multi body dynamics C++ library [31]. As in the Fortran implementation of [25], the time integration method is stable even under large time steps, and the user has to set just the mass and friction parameters of the material. It should be remarked that modeling masonry blocks as perfectly rigid contacts may seem idealized, but it does not decrease the quality of the model. In fact, for the reasons mentioned earlier, stiffness and damping laws are affected by local complex geometric and rheological phenomena, that cannot be assessed, even limiting to average physical values, without an *ad hoc* experimental research on its own. Moreover, even the most classical solution for linear elastic bodies under concentrated contact forces suffers from intrinsic inconsistencies [17]. To our knowledge, only recently the NSCD formulation for rigid blocks has started to be successfully applied to the study of old, possibly deteriorated, masonry construction [29], but many variations are possible within this broad class of models.

Especially, the friction law used in the proposed approach deserves further comments. According to experimental results [50, 9], friction is slightly associative because of roughness of the contact profiles, i.e., a normal displacement (dilatancy) accompanies sliding across the frictional surface [18]. However, it is clear since the work by Drucker [14] that sliding in the presence of friction *à la* Coulomb invalidates the general bounding theorems of plasticity, since the normality rule is not fulfilled. The formulation of the problem is complicated, and a right failure load may be associated with an incorrect failure mode [21]. Our approach includes set-valued force laws and complementarity constraints as required by the original Coulomb contact model. This is formulated as a Differential Variational Inequality (DVI). As such, DVIs impose constraints in the form of Variational Inequalities (VI) during the time evolution of the system [38, 37]. Such set-valued functions can be expressed by the same MDI theory.

A common issue in NSCD methods as applied to masonry structures [15, 28, 41] is the multiplicity of solutions for the contact forces, especially in the tangential direction. This is a natural consequence of the rigid body idealization, although it often does not affect the uniqueness of solutions for speeds and trajectories. Here, we introduce a regularization that ensures uniqueness even for contact forces, resulting in better numerical performance of the time-stepping algorithm and in improved clarity of the plotted results.

When one deals with architectural complex masonry structures, not only the simulation time, but even the geometrical definition of blocks and the communicability of the results can be a problem. This is why we have integrated our computational software with a userfriendly design tool. We used the Grasshopper@ free parametric design plug-in for the Rhino@ CAD software, both to generate and modify the geometry of the source data and to post-process the computational results. With such a tool we provide the real-time visualization of forces, stress and collapse mechanisms, and displays the *effective* thrust line in arches, as the envelope curve of the resultant of the contact forces at the blocks interfaces.

The plan of the article is as follows. In Section 2 we present the proposed method and its numerical implementation, with special focus on the contact frictional model. In Section 3, the potentiality of the method is highlighted through the analysis of representative case studies. The efficiency of the computations is addressed in Section 4, where we study the response to dynamic loads. The overall achievements, drawbacks and further developments are discussed in the concluding Section 5.

2 Non-smooth contact dynamics

In a classical ODE or DAE, one assumes smooth speeds and accelerations. However, the introduction of hard contacts leads to non-smooth trajectories, and this requires a NSCD framework based on MDI, that encompasses jumps in speeds. In a MDI, acceleration is not a function in a classical sense because, as a consequence of impact events and other impulsive phenomena, it contains a certain number of spikes, which can be considered using the theory of (vector signed) measure distributions. In detail, positions $\boldsymbol{q}(t)$ are *Absolutely Continuous* (AC) functions but speeds $\boldsymbol{v}(t)$ are *functions of Bounded Variation* (BV), with finite variation $\bigvee_{t_a}^{t_b} \boldsymbol{v}(t)$ for $[t_a, t_b] \subset [0, T]$, i.e., they do not need to be absolutely continuous or even continuous.

Before proceeding with the mathematical model of our NSCD problem, we need to introduce some definitions.

Definition 1 *A Variational Inequality VI($\boldsymbol{F}, \mathcal{K}$) is a problem of the type*

$$\boldsymbol{x} \in \mathcal{K} \quad : \quad \langle \boldsymbol{F}(\boldsymbol{x}), \boldsymbol{y} - \boldsymbol{x} \rangle \geq 0 \quad \forall \boldsymbol{y} \in \mathcal{K}, \tag{1}$$

with $\mathcal{K}$ closed and convex, and $\boldsymbol{F}(\boldsymbol{x}) : \mathcal{K} \to \mathbb{R}^n$ continuous.

Definition 2 *The dual cone $\mathcal{K}^*$ of $\mathcal{K}$ is a convex cone expressed as:*

$$\mathcal{K}^* = \{\boldsymbol{y} \in \mathbb{R}^n : \langle \boldsymbol{y}, \boldsymbol{x} \rangle \geq 0 \quad \forall \boldsymbol{x} \in \mathcal{K}\}\,. \tag{2}$$

Definition 3 *A Cone Complementarity Problem CCP($A, \boldsymbol{b}, \Upsilon$) is the problem of finding a $\boldsymbol{x}$ that satisfies*

$$A\boldsymbol{x} - \boldsymbol{b} \in \Upsilon^*, \quad \boldsymbol{x} \in \Upsilon, \quad \langle A\boldsymbol{x} - \boldsymbol{b}, \boldsymbol{x} \rangle = 0, \tag{3}$$

where Υ is a (convex) cone. One can also use the notation $A\boldsymbol{x} - \boldsymbol{b} \in \Upsilon^* \perp \boldsymbol{x} \in \Upsilon$. The CCP is equivalent to a VI where $\mathcal{K} = \Upsilon$ and with affine $\boldsymbol{F}$.

2.1 System state

For each $i-$th block in the system, we introduce the position $\boldsymbol{x}_i \in \mathbb{R}^3$ of its center of mass, and we introduce its rotation matrix $A_i \in \mathsf{SO3}$, both expressed relatively to the absolute reference. To avoid redundant parameters, we parametrize $\mathsf{SO3}$ using its double cover S^3, the hypersphere of unit-length quaternions, i.e. $\mathbb{H}_1$. The quaternion that expresses the rotation of the i-th block is then $\boldsymbol{\rho}_i \in \mathbb{H}_1$, a set of four scalars. We recall that one can convert between both matrix or quaternion representations of rotation when needed: $A = A(\boldsymbol{\rho})$ and $\boldsymbol{\rho} = \boldsymbol{\rho}(A)$. The velocity of the $i-$th block is expressed with a vector $\dot{\boldsymbol{x}}_i \in \mathbb{R}^3$, considered in the absolute reference system. The angular velocity of the $i-$th block is a vector $\boldsymbol{\omega}_i \in \mathbb{R}^3$, expressed in the body-local coordinates.

The state of the system at time t is represented by generalized coordinates $\boldsymbol{q}(t) \in \mathbb{R}^{m_q}$ and by generalized velocities $\boldsymbol{v}(t) \in \mathbb{R}^{m_v}$:

$$\boldsymbol{q} = \{\boldsymbol{x}_1^T, \boldsymbol{\rho}_1^T, \boldsymbol{x}_2^T, \boldsymbol{\rho}_2^T, ...\}^T\,, \tag{4}$$

$$\boldsymbol{v} = \{\dot{\boldsymbol{x}}_1^T, \boldsymbol{\omega}_1^T, \dot{\boldsymbol{x}}_2^T, \boldsymbol{\omega}_2^T, ...\}^T\,. \tag{5}$$

2.2 Contacts

Under the assumption of perfectly rigid bodies, unilateral contacts lead to complementarity constraints. We introduce a set of $\mathcal{G}_\mathcal{A}$ contact constraints between pairs of shapes. For each contact constraint we assume that there is a signed distance function

$$\Phi_i(\boldsymbol{q}) \geq 0\,, \tag{6}$$

differentiable in $\boldsymbol{q}$.

Some remarks need to be made here.

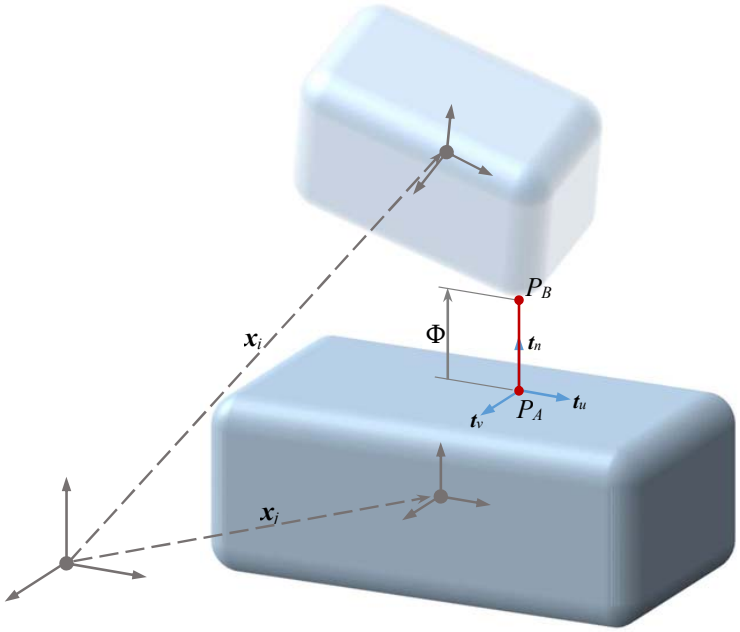

Figure 1: The signed distance function for a couple of collision shapes.

- Each $\Phi_i(\boldsymbol{q})$ corresponds to a *couple of nearest contact points*, that should be coincident, $\Phi_i(\boldsymbol{q}) = 0$,when the contact is active, or separated, $\Phi_i(\boldsymbol{q}) > 0$, when the contact is inactive as for approaching or departing motion of two surfaces, as shown in Figure 1.

- The set $\mathcal{G}_\mathcal{A}$ varies continuously during the simulation, as the collision detection engine adds, removes or updates contacts at each time step.

- A contact constraint should be added to the $\mathcal{G}_\mathcal{A}$ set before the surfaces start to interpenetrate and the contact is likely to happen within one time step. However, adding it when the two bodies are still too far apart will create too many superfluous contact constraints, resulting in a computational burden. Thus, in our code we add a contact pair to the $\mathcal{G}_\mathcal{A}$ manifold only when $\Phi_i(\boldsymbol{q}) < \epsilon_e$, where ϵ_e is an user defined tolerance.

- The differentiability of $\Phi_i(\boldsymbol{q})$ does not hold in general, e.g., when considering sharp edges in G^0 surfaces. Nevertheless, while assuming the couple of nearest contact points to be fixed to the surfaces for small motions, this is not an issue.

- The case $\Phi_i(\boldsymbol{q}) < 0$ shall never happen, since (6) enforces the opposite, but for various reasons including numerical inaccuracies or wrong initial conditions, this might still happen. Therefore, we developed our numerical method in order to cope also with this situation, for the sake of algorithmic robustness.

- Even a single pair of rigid bodies could lead to *multiple* contacts. In the case of two smooth convex shapes, most notably the case of sphere vs. sphere, it is easy to compute a single distance function $\Phi_i(\boldsymbol{q})$, but difficulties arise when one or both of the two shapes is concave. Also faceted convex shapes (convex hulls, boxes, etc.) can pose difficulties with degenerate cases, for instance when two faces are coplanar or an edge is coplanar to a face. In sake of performance, all these situations are cast as a set of multiple contact points between the two shapes, although this process is demanded to the heuristics of the collision detection algorithm. Our algorithm tends to create the smallest amount of required contact pairs.

For a perfectly rigid contact, the Signorini condition leads to the complementarity constraint

$$\Phi_i(\boldsymbol{q}) \geq 0 \perp \widehat{\gamma}_{n,i} \geq 0\,, \tag{7}$$

that states the requirement that $\widehat{\gamma}_{n,i}$ is positive when the distance is null (active contact) and, *vice versa*, the distance is positive only when $\widehat{\gamma}_{n,i}$ is null.

A local coordinate system with one normal $\boldsymbol{t}_{n,i} \in \mathbb{R}^3$ and two mutually orthogonal tangents $\boldsymbol{t}_{u,i}, \boldsymbol{t}_{v,i} \in \mathbb{R}^3$ axes can be computed at each contact point. The normal force value is expressed by a multiplier $\widehat{\gamma}_{n,i}$.

Similarly, we introduce the force multipliers $\widehat{\gamma}_{u,i}, \widehat{\gamma}_{v,i}$ for the tangential forces caused by friction. The contact force in 3D space, in its normal $\boldsymbol{F}_{n,i}$ and tangential component $\boldsymbol{F}_{\parallel,i}$, is thus

$$\begin{aligned} \boldsymbol{F}_i &= \boldsymbol{F}_{n,i} + \boldsymbol{F}_{\parallel,i} && (8)\\ &= \widehat{\gamma}_{n,i}\boldsymbol{t}_{n,i} + \widehat{\gamma}_{u,i}\boldsymbol{t}_{u,i} + \widehat{\gamma}_{v,i}\boldsymbol{t}_{v,i}\,. && (9) \end{aligned}$$

We introduce also the speeds at the contact point, both in normal $\boldsymbol{v}_{n,i}$ and tangential component $\boldsymbol{v}_{\parallel,i}$. These are related to generalized velocities $\boldsymbol{v} \in \mathbb{R}^{n_v}$ *via* the Jacobians $\boldsymbol{D}_{n,i}, \boldsymbol{D}_{u,i}, \boldsymbol{D}_{v,i}$ in the form

$$\begin{aligned} \mathbf{v}_i &= \mathbf{v}_{n,i} + \mathbf{v}_{\parallel,i} && (10)\\ &= u_{n,i}\boldsymbol{t}_{n,i} + u_{u,i}\boldsymbol{t}_{u,i} + u_{v,i}\boldsymbol{t}_{v,i} && (11)\\ &= (\boldsymbol{D}_{n,i}^T\boldsymbol{v})\boldsymbol{t}_{n,i} + (\boldsymbol{D}_{u,i}^T\boldsymbol{v})\boldsymbol{t}_{u,i} + (\boldsymbol{D}_{v,i}^T\boldsymbol{v})\boldsymbol{t}_{v,i}\,. && (12) \end{aligned}$$

The Coulomb-Amontons contact model, as shown in Figure 2, introduces the friction coefficient μ_i and states that $\mu\widehat{\gamma}_{n,i} \geq \sqrt{\widehat{\gamma}_{u,i}^2 + \widehat{\gamma}_{v,i}^2}$ for $\widehat{\gamma}_{n,i} \in \mathbb{R}^+$, and that the tangential velocity at contact $\left|\left|\mathbf{v}_{\parallel}\right|\right|$ are in opposite direction, i.e. $\left\langle \boldsymbol{F}_{\parallel}, \mathbf{v}_{\parallel} \right\rangle = -\left|\left|\boldsymbol{F}_{\parallel}\right|\right| \left|\left|\mathbf{v}_{\parallel}\right|\right|$.

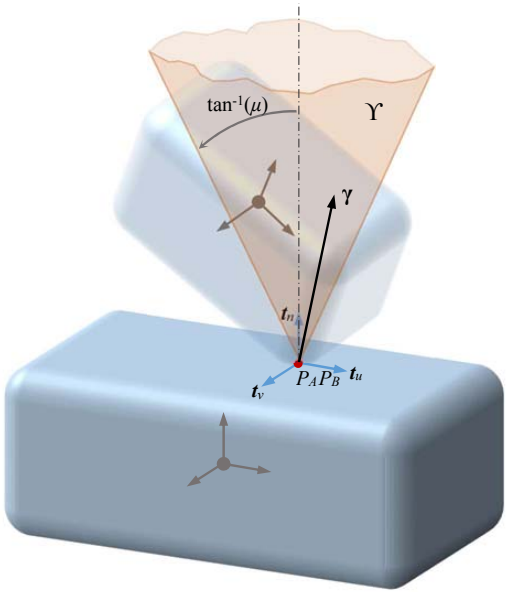

Figure 2: The Coulomb friction cone for a single contact.

This can be reformulated using an optimization constraint, expressed by the maximum dissipation principle [47, 44, 45]

$$(\widehat{\gamma}_u, \widehat{\gamma}_v) = \text{argmin}_{\sqrt{\widehat{\gamma}_u^2+\widehat{\gamma}_v^2} \leq \mu \widehat{\gamma}_n} \left(\widehat{\gamma}_u \boldsymbol{t}_1 + \widehat{\gamma}_v \boldsymbol{t}_2\right)^T \mathbf{v}_{\parallel}. \tag{13}$$

We remark that the contact model of (13) depends only on a constant parameter μ_i. Differently to the original Coulomb-Amontons model, we do not make distinction between static $\mu_{i,s}$ and kinetic $\mu_{i,k}$ friction coefficients. In many scenarios involving dry friction it happens that $\mu_{i,k}$ is a bit lower than $\mu_{i,s}$, as sticking in general allows a slightly superior margin of tangential adhesion with respect to the case of sliding. With some changes, our formulation could also support this distinction $\mu_{i,s} \neq \mu_{i,k}$ and even more sophisticated cases such as the Stribeck effect, where $\mu_i = \mu_i(\mathbf{v}_{\parallel,i})$, but in the following we will assume $\mu_i = \mu_{i,s}$ for simplicity. In our tests, given that the sliding speed between the blocks is null (in the case of static analysis) or moderate (in the case of transient seismic analysis), the Stribeck effect would have no significant impact on the outcome and can be neglected.

For active contacts, i.e., those with $\Phi = 0$, Eq. (7) can be formulated also at the speed level as $\dot{\Phi}_i(\boldsymbol{q}) \geq 0 \perp \widehat{\gamma}_{n,i} \geq 0$, with $\dot{\Phi}_i(\boldsymbol{q}) = u_{n,i} = \boldsymbol{D}_{n,i}\boldsymbol{v}$. Then, using the De Saxcé-Feng bipotential [43] one can write the maximum dissipation principle of (13) as a cone complementarity. To this end one we introduce the second order Lorentz cones

$$\Upsilon_i = \left\{ \widehat{\gamma}_n, \widehat{\gamma}_u, \widehat{\gamma}_v \mid \mu_i \widehat{\gamma}_n \geq \sqrt{\widehat{\gamma}_u^2 + \widehat{\gamma}_v^2} \right\} \quad \subset \mathbb{R}^3 \,,$$

and their dual cones $\Upsilon_i^* = \{\widehat{\boldsymbol{\gamma}} | \langle \widehat{\boldsymbol{\gamma}}, \boldsymbol{x} \rangle \geq 0 \quad \forall \boldsymbol{x} \in \Upsilon_i\}$, so that (13) can be written as a cone complementarity problem

$$\widehat{\boldsymbol{\gamma}}_i \in \Upsilon_i \perp \bar{\boldsymbol{u}}_i \in \Upsilon_i^*, \quad \forall i \in \{\mathcal{G}_\mathcal{A}, \Phi_i = 0\}, \tag{14}$$

where we introduced

$$\widehat{\boldsymbol{\gamma}}_i = \left\{ \begin{array}{l} \widehat{\gamma}_{u,i} \\ \widehat{\gamma}_{v,i} \\ \widehat{\gamma}_{n,i} \end{array} \right\}, \tag{15}$$

and

$$\bar{\boldsymbol{u}}_i = \left\{ \begin{array}{l} u_{n,i} + \mu_i \sqrt{u_{u,i}^2 + u_{v,i}^2} \\ u_{u,i} \\ u_{v,i} \end{array} \right\} \tag{16}$$

$$= D_i^T \boldsymbol{v} + \left\{ \begin{array}{l} \mu_i \left|\left| D_{\|,i}^T \boldsymbol{v} \right|\right| \\ 0 \\ 0 \end{array} \right\} \tag{17}$$

$$= \boldsymbol{u}_i + \tilde{\boldsymbol{u}}_i . \tag{18}$$

Here we used the matrices $D_i \in \mathbb{R}^{m_v \times 3}$ and $D_{\|,i} \in \mathbb{R}^{m_v \times 2}$, as

$$D_i = [\boldsymbol{D}_{n,i} | \boldsymbol{D}_{u,i} | \boldsymbol{D}_{v,i}] = \left[\boldsymbol{D}_{n,i} | D_{\|,i}\right] . \tag{19}$$

2.3 The complete dynamical model

We introduce the generalized forces $\boldsymbol{f}(\boldsymbol{q}, \boldsymbol{v}, t) \in \mathbb{R}^{m_v}$, including gravitational forces, external applied forces, gyroscopic forces. The block-diagonal mass matrix $M \in \mathbb{R}^{m_q \times m_q}$ contains all the masses and inertia tensors of the rigid bodies. Therefore, the complete multibody problem can be formulated as

$$M \frac{d\boldsymbol{v}}{dt} = \boldsymbol{f}(\boldsymbol{q}, \boldsymbol{v}, t) + \sum_{i \in \mathcal{G}_\mathcal{A}} D_i \widehat{\boldsymbol{\gamma}}_i(t), \tag{20}$$

$$\widehat{\boldsymbol{\gamma}}_i \in \Upsilon_i \perp \bar{\boldsymbol{u}}_i \in \Upsilon_i^* \quad \forall i \in \{\mathcal{G}_\mathcal{A} | \Phi_i = 0\}, \tag{21}$$

$$\dot{\boldsymbol{q}} = \Gamma(\boldsymbol{q}) \boldsymbol{v} . \tag{22}$$

At this point, we need a time integration algorithm that can solve Equations (20)-(22). One might be tempted to solve for unknown acceleration $\frac{d\boldsymbol{v}}{dt}$ and unknown reaction forces

$\widehat{\boldsymbol{\gamma}}_i$ at discrete time steps. Although this is possible (and could also work in some cases), it is known that there are problems that can be solved only by endorsing the MDI framework, where speeds are functions of bounded variations [36][48]. In order to accommodate discontinuous events, numerical methods for MDIs approximate $\boldsymbol{q}(t)$ and $\boldsymbol{v}(t)$ with discrete values $\boldsymbol{q}_n(t)$ and $\boldsymbol{v}_n(t)$ where $\boldsymbol{q}_n(t) \to \boldsymbol{q}(t)$ uniformly and $\boldsymbol{v}_n(t) \to \boldsymbol{v}(t)$ pointwise (i.e. with *weak** convergence of the differential measures $d\boldsymbol{v}_n \overset{*}{\rightharpoonup} d\boldsymbol{v}$). The weak* convergence of MDIs and the $h \downarrow 0$ convergence of time stepping schemes based on MDIs are discussed in [46].

From a practical perspective, the MDI approach leads to time stepping schemes where the unknowns at each time steps are measures $(\boldsymbol{v}^{(l+1)} - \boldsymbol{v}^{(l)})$ over a time step h, and reaction impulses $\boldsymbol{\gamma}_i = \int_t^{t+h} d\boldsymbol{\gamma}_i(dt)$, where the vector signed Radon measure $d\boldsymbol{\gamma}_i$ can be decomposed as $d\boldsymbol{\gamma}_i = \widehat{\boldsymbol{\gamma}}_i(t)dt + \boldsymbol{\xi}_i$, including continuous forces $\widehat{\boldsymbol{\gamma}}_i(t) \in L^1$ over Lebesgue dt and impulses expressed by atomic measures $\boldsymbol{\xi}_i$ that generate instantaneous changes in velocity.

2.4 The time stepping method

We present a time stepping method for the solution of the MDI, inspired by the scheme developed in [47]. For a more compact notation, we introduce the following system-level terms:

$$D = [D_1 \mid ... \mid D_{n_\mathcal{A}}], \tag{23}$$

$$\boldsymbol{\gamma} = [\boldsymbol{\gamma}_1 \mid ... \mid \boldsymbol{\gamma}_{n_\mathcal{A}}], \tag{24}$$

$$\bar{\boldsymbol{u}} = [\bar{\boldsymbol{u}}_1 \mid ... \mid \bar{\boldsymbol{u}}_{n_\mathcal{A}}], \tag{25}$$

$$\Upsilon = \left(\bigtimes_{i \in \mathcal{G}_\mathcal{A}} \Upsilon_i \right), \quad \Upsilon^* = \left(\bigtimes_{i \in \mathcal{G}_\mathcal{A}} \Upsilon_i^* \right). \tag{26}$$

Since the integration process is affected by various numerical inaccuracies (integration error, finite precision of floating point, etc.) it might happen that errors accumulate and constraints would show a gradual drift from the zero-residual condition. This means that contacts could start to interpenetrate gradually after many integration steps, even if contact conditions are satisfied exactly at the speed level. This can be solved by introducing a stabilization term that keeps constraints and contacts satisfied also at the position level [3]. To this end, we introduce the stabilization term $\boldsymbol{b}$ in $\underline{\bar{\boldsymbol{u}}}^{(l+1)} = \bar{\boldsymbol{u}}^{(l+1)} + \boldsymbol{b}$, where

$$\boldsymbol{b} = \left[\frac{1}{h}\Phi_1|0|0 \mid ... \mid \frac{1}{h}\Phi_{n_\mathcal{A}}|0|0 \right]. \tag{27}$$

Finally, for a time step h, one can rewrite Equations (20)-(22) in discrete form to obtain the following problem to be solved when advancing from time step $t^{(l)}$ to time step $t^{(l+1)}$, using impulses $\boldsymbol{\gamma}$:

$$\boldsymbol{\gamma} \in \Upsilon \perp \bar{\underline{\boldsymbol{u}}}^{(l+1)} \in \Upsilon^* \,, \tag{28}$$

$$M^{(l)}(\boldsymbol{v}^{(l+1)} - \boldsymbol{v}^{(l)}) = \boldsymbol{f}(\boldsymbol{q}^{(l)}, \boldsymbol{v}^{(l)}, t^{(l)})h + D^{(l)}\boldsymbol{\gamma}(t) \,, \tag{29}$$

$$\boldsymbol{q}^{(l+1)} = \Theta(\boldsymbol{q}^{(l)}, \boldsymbol{v}^{(l+1)}) \,. \tag{30}$$

We remark that such time stepping method consists in the following three phases, which can be solved in sequence, at each time step.

- Unknown impulses $\boldsymbol{\gamma}$ are computed from the CCP of (28); this is the main computational bottleneck of the entire simulation, taking up to 90% of the CPU time; this involves complex computations that will be discussed more in detail in the following paragraphs.
- Unknown new speeds $\boldsymbol{v}^{(l+1)}$ are computed in (29); this would require the solution of a linear system with a large M matrix but, given its block-diagonal structure, the M^{-1} matrix is immediate to calculate.
- New positions $\boldsymbol{q}^{(l+1)}$ are computed from $\boldsymbol{q}^{(l)}$ and $\boldsymbol{v}^{(l+1)}$ with a first-order integration; if we had only translations, the $\Theta(\cdot)$ mapping would turn into the Euler-Cromer semi implicit update $\boldsymbol{q}^{(l+1)} = \boldsymbol{q}^{(l)} + h\boldsymbol{v}^{(l+1)}$; however, we have $m_q \neq m_v$ because we use quaternions to parametrize rotations, so we use the standard update only for $\boldsymbol{x}_i$ terms, whereas we use the exponential map of pure-imaginary quaternions to update the rotations, i.e.,

$$\boldsymbol{q}^{(l+1)} = \Theta(\boldsymbol{q}^{(l)}, \boldsymbol{v}^{(l+1)}) = \left\{ \begin{array}{l} \boldsymbol{x}_1^{(l)} + h\dot{\boldsymbol{x}}_1^{(l+1)} \\ \boldsymbol{\rho}_1^{(l)} \exp(\{0, \frac{1}{2}\boldsymbol{\omega}_1^{(l+1)} h\}) \\ \boldsymbol{x}_2^{(l)} + h\dot{\boldsymbol{x}}_2^{(l+1)} \\ \boldsymbol{\rho}_2^{(l)} \exp(\{0, \frac{1}{2}\boldsymbol{\omega}_2^{(l+1)} h\}) \\ \ldots \end{array} \right\} .$$

An interesting remark is that the method of (28)-(30) solves dynamical problems such as those arising by seismic transient analysis or collapses, but in a less general setting, the same formulation (28)-(29) can be used to solve a static analysis as a special case. In fact, a static analysis can be achieved with a single solution of the CCP with arbitrary h and with $\boldsymbol{v}^{(l)} = \boldsymbol{0}$, a highly non-linear complementarity problem whose solution gives $\boldsymbol{v}^{(l+1)}$ and contact forces $h\boldsymbol{\gamma}$. Once such CCP is solved, one checks if $||\boldsymbol{v}^{(l+1)}|| = 0$ is verified: if so, by definition, there is a static solution; otherwise $||\boldsymbol{v}^{(l+1)}|| > 0$ means that the initial configuration cannot withstand the $\boldsymbol{f}(\boldsymbol{q}, \boldsymbol{v}, t)$ load, that is, blocks would move and possibly collapse.

Now, consider the CCP of (28). This problem can be transformed in a form that fits better in a computational framework. From (16), one sees that local contact and constraints

speeds are function of generalized speeds, $\underline{\bar{\boldsymbol{u}}}^{(l+1)} = \underline{\bar{\boldsymbol{u}}}(\boldsymbol{v}^{(l+1)})$, as well as (28) shows that generalized speeds are function of reactions, i.e., $\boldsymbol{v}^{(l+1)} = \boldsymbol{v}(\boldsymbol{\gamma})$; so we aim at expressing $\underline{\bar{\boldsymbol{u}}}^{(l+1)} = \underline{\bar{\boldsymbol{u}}}(\boldsymbol{\gamma})$.

Introducing

$$\tilde{\boldsymbol{k}}^{(l)} = M^{(l)}\boldsymbol{v}^{(l)} + h\boldsymbol{f}_t(\boldsymbol{q}^{(l)}, \boldsymbol{v}^{(l)}, t^{(l)}),$$

and premultiplying Equation (29) by ${M^{(l)}}^{-1}$, one gets

$$\boldsymbol{v}^{(l+1)} = {M^{(l)}}^{-1} D\boldsymbol{\gamma} + {M^{(l)}}^{-1}\tilde{\boldsymbol{k}}. \tag{31}$$

By substitution of $\boldsymbol{v}^{(l+1)}$ of (31) in (16), one has

$$\underline{\bar{\boldsymbol{u}}}^{(l+1)} = D^T {M^{(l)}}^{-1} D\boldsymbol{\gamma} + D^T {M^{(l)}}^{-1}\tilde{\boldsymbol{k}} + \boldsymbol{b} + \tilde{\boldsymbol{u}}(\boldsymbol{v}^{(l+1)})\,. \tag{32}$$

To make the expressions more compact, we introduce the Delassus operator N and the vector $\boldsymbol{r}$ in the form

$$N = D^T {M^{(l)}}^{-1} D\,, \tag{33}$$

$$\boldsymbol{r} = D^T {M^{(l)}}^{-1}\tilde{\boldsymbol{k}} + \boldsymbol{b}\,, \tag{34}$$

so to obtain

$$\underline{\bar{\boldsymbol{u}}} = N\boldsymbol{\gamma} + \boldsymbol{r} + \tilde{\boldsymbol{u}}(\boldsymbol{v}^{(l+1)})\,. \tag{35}$$

We note that the $\tilde{\boldsymbol{u}}(\boldsymbol{v}^{(l+1)})$ term is a non-linear function of $\boldsymbol{v}^{(l+1)}$, i.e., it is also a nonlinear function of $\boldsymbol{\gamma}$. Therefore, equation (28) becomes the non-linear complementarity problem

$$\boldsymbol{\gamma} \in \Upsilon \perp \underline{\bar{\boldsymbol{u}}}(\boldsymbol{\gamma}) \in \Upsilon^*\,. \tag{36}$$

As such, not only it is difficult to prove existence and uniqueness of the solution, but major numerical difficulties arise when one attempts at solving it.

In [2] it has been demonstrated that one can make the problem convex by neglecting the $\tilde{\boldsymbol{u}}$ term, at the cost of accepting that the friction model become associated. As shown in [5], this has the side effect that, during sliding motion, a small gap proportional to $h\left|\left|\mathbf{v}_{i,\|}\right|\right|\mu_i$ builds up, but it does not increase any further, because of the Φ/h term that we added for stabilization. This can be seen as a dilatation effect, whose magnitude tends to zero or negligible values as the tangential sliding speed $\mathbf{v}_{i,\|}$ is small (something that easily fits in simulations of falling or stacked building blocks, for instance) or for small friction coefficients μ_i, or for $h \downarrow 0$.

If the $\tilde{\boldsymbol{u}}$ term is dropped, one can introduce $\underline{\boldsymbol{u}} = \boldsymbol{u} + \boldsymbol{b}$ as a simplified version of the $\bar{\underline{\boldsymbol{u}}}$ term, which now becomes an affine function of $\boldsymbol{\gamma}$ of the type

$$\underline{\boldsymbol{u}} = N\boldsymbol{\gamma} + \boldsymbol{r}\,. \tag{37}$$

Then, equation (36) becomes a second-order convex CCP$(N, \boldsymbol{r}, \Upsilon)$ of the form

$$\boxed{\boldsymbol{\gamma} \in \Upsilon \perp N\boldsymbol{\gamma} + \boldsymbol{r} \in \Upsilon^*\,.} \tag{38}$$

We have seen that a CCP$(N, \boldsymbol{r}, \Upsilon)$ is a special case of a VI$(\boldsymbol{F}, \Upsilon)$ with affine $\boldsymbol{F}$, and it is known that such VI is also equivalent to the convex program [26]

$$\boxed{\begin{aligned} \boldsymbol{\gamma} = &\operatorname{argmin}\ \boldsymbol{\gamma}^T N\boldsymbol{\gamma} + \boldsymbol{\gamma}^T\boldsymbol{r} && (39)\\ &\text{s.t.}\quad \boldsymbol{\gamma} \in \Upsilon\,. && (40) \end{aligned}}$$

We designed different numerical methods in order to solve the CCP of (38) or of (40).

One option is the fixed-point iteration presented in [5]. It is a variant of the Gauss-Seidell stationary iteration, endowed with separable projections on Υ. This method features algorithmic robustness and it is easy to implement; however it is affected by stall in convergence in scenarios where there are long sequences of objects in contact, that is exactly what happens in many problems of engineering interest, such as a stack of blocks.

In sake of a better convergence property, in a previous work [24] we also developed the P-SPG-FB method, a variant of the non-monotone Spectral Projected Gradient method [8] that features diagonal preconditioning and a fall-back strategy to ensure monotone convergence. The P-SPG-FB method operates a minimization of a function over separable convex constraints, so to exploit the formulation of the problem in the form of (40). This is the method of choice for the simulations reported in this paper.

2.5 Contact detection

Computing the $\mathcal{G}_{\mathcal{A}}$ set of contact points is a non trivial task. A first difficulty stems from the fact that we cannot compute contacts for all possible pairs of blocks in the simulation, as this would lead to an algorithm with $O(n^2)$ complexity class. This could be tolerated only for problems involving few blocks, but it would easily become a bottleneck for larger scenarios even with few hundreds of bricks, especially considering that the collision detection is performed at each time step. For this reason, our collision pipeline is split in two phases: a *broad phase* that sorts out only those pairs of blocks that are close enough and that could potentially generate some contact points, and a successive *narrow phase* that focuses on those pairs, by refining one or more contact points between them.

In the literature there are various methods for performing the broad phase filtering. We adopted a bounding volume hierarchy, a data structure based on a dynamic tree of Axis Aligned Bounding Boxes (AABB) as implemented in [11]. This algorithm is very efficient and outputs a list of blocks whose bounding boxes are overlapping. In general for masonry-like structures the amount of those potential collision pairs n_{cp} is proportional to the number of blocks, $n_{cp} = K_{cp} n$ with a small K_{cp} usually in the range 1...6, so that the entire collision algorithm tends to a $O(n)$ complexity.

The narrow phase stage operates on the pairs of blocks being selected by the previous broad phase. The method that we use is based on the Gilbert-Johnson-Keerthi GJK algorithm [16], that returns a couple of nearest points between a pair of convex shapes. The GJK algorithm is fast and operates on whatever kind of convex surface (boxes, faceted polytopes, cylinders, etc.), but we had to address two issues.

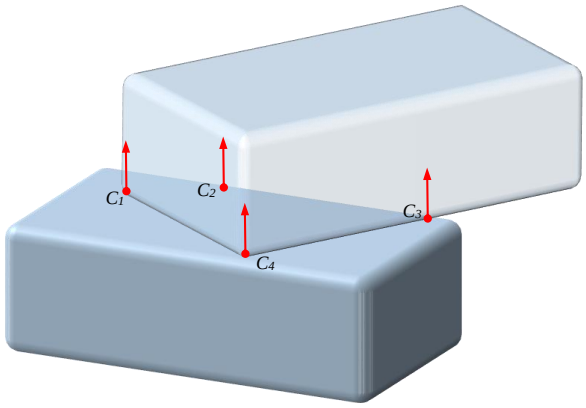

Figure 3: Multiple contact points between coplanar facets.

The first problem is represented by the fact that one might have degenerate cases where two faces are coplanar, and multiple contact points should be returned, whereas GJK would return just a single contact point. This issue is solved by running the GJK algorithm multiple times with small perturbations on object rotations, thus obtaining points in multiple positions. Then, an heuristic collision filtering step would remove unnecessary contacts by keeping only those that maximize the contact patch (Figure 3).

The second problem is related to the fact that the GJK algorithm assumes shapes to be separated, but as we said previously, the time integration might not be able to prevent slight interpenetration between some blocks. In fact, a precise $\Phi = 0$ value cannot be ensured for active contacts, as numerical inaccuracy rather leads to small oscillations around the zero value. To overcome this difficulty, we implemented a workaround that enhances the robustness of the GJK algorithm even in case of small penetrations. As shown in Figure 4, the idea is to consider the original shapes as sphere-swept surfaces, i.e., Minkowski sums of two smaller shapes and two spheres with diameter ϵ_m, then the GJK algorithm is run on

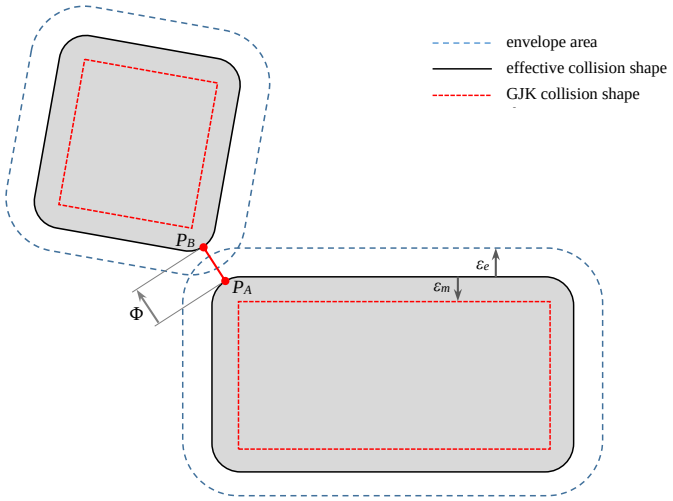

Figure 4: Collision shapes and tolerances.

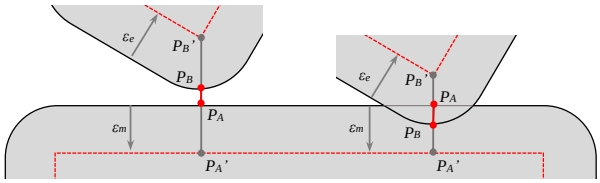

Figure 5: Robust handling of small penetrations using sphere-swept surfaces.

the smaller, shrunk shapes. When the nearest contact points P'_A and P'_B are found between the shrunk shapes, we offset them along the normal by a quantity ϵ_m, to obtain P_A and P_B, that are sent to the $\mathcal{G}_A$ set. In this way, the multibody solver operates on P_A and P_B, rather than on P'_A and P'_B. Hence we can accept penetrations with negative distance up to $2\epsilon_m$ between P_A and P_B, while P'_A and P'_B are still separated with positive distance, something that ensures the robustness of the GJK algorithm (see Figure 5). The only drawback of this approach is that one must pre-process the original shapes of the blocks in order to generate the inset shrunk shapes (something that can be done with the algorithm presented in [40]) and that the collision points do not follow the original shape at the corners, because sharp corners get a fillet[1] of radius ϵ_m.

[1]Far from being a shortcoming, the presence of fillets on the corners of collision shapes is consistent in our problem involving architectural masonry, as stone blocks and bricks are never perfectly sharp, and most often they are rounded and smoothed at the corners.

2.6 Regularization

Existence and uniqueness of the solution to the original CCP problem of Equation (38) holds only under special circumstances.

The convex relaxation that we introduced by assuming an associated friction law has little or no importance in the case of static problems, because the $\boldsymbol{v} = \mathbf{0}$ case is a sufficient condition[2] for the term $\tilde{\boldsymbol{u}}$ to vanish in (37). This said, we can develop results about existence and uniqueness in the static regime by studying the convex program of Equation (40). To this end we introduce some concepts.

Definition 4 *The Generalized Friction Cone $\mathcal{Y}_\Upsilon$ is a convex cone defined as*

$$\mathcal{Y}_\Upsilon = \left\{ \boldsymbol{f}_c = \sum_{i \in \mathcal{G}_{\mathcal{A}*}} D_i \widehat{\boldsymbol{\gamma}}_i \middle| \widehat{\boldsymbol{\gamma}}_i \in \Upsilon_i, \forall i \in \mathcal{G}_{\mathcal{A}*} \right\}, \tag{41}$$

where $\mathcal{G}_{\mathcal{A}*} \subset \mathcal{G}_{\mathcal{A}}$ is the set of active contacts with $\Phi_i = 0$.

Following [4], one can show that under some assumptions on the regularity of $\mathcal{Y}_\Upsilon$, there is an unique solution in terms of the dual variables $\boldsymbol{\gamma}$. This requires the following

Definition 5 *The Pointed Friction Cone Constraint Qualification (PFCCQ) means*

$$\mathcal{Y}_\Upsilon \text{ satisfies PFCCQ} \Leftrightarrow \left\{ \forall (\widehat{\boldsymbol{\gamma}}_i \in \Upsilon_i) \neq \mathbf{0}, \forall i \in \mathcal{G}_{\mathcal{A}*}, \text{ it must be } \sum_{i \in \mathcal{G}_{\mathcal{A}*}} D_i \widehat{\boldsymbol{\gamma}}_i \neq \mathbf{0} \right\}. \tag{42}$$

Equivalently this means that there are no combinations of non-zero constraint multipliers (that fit the Coulomb cones) whose net effect is zero in terms of generalized torques/forces.

However it is easy to see that such constraint qualification does not hold in general for the problems presented in this paper. It is sufficient to take a counter-example: a rigid body stacked on top of a table, at rest, touching the table in three points. In such a case, one could prove that there are infinitely many solutions for the tangential reactions at the three contact point, provided that they cancel out in horizontal direction. Adding further contact points between two rigid bodies leads to even more over-constrained problems. Effectively, it is impossible to build a practical model of a 3D structure made by rigid blocks that satisfies PFCCQ.

[2] More precisely a necessary and sufficient condition for $\tilde{\boldsymbol{u}} = \mathbf{0}$ is that all contacts are all sticking or rolling without slip. The all-sticking sub case is implied by $\boldsymbol{v} = 0$.

It is interesting to remark that this multiplicity of solutions in terms of dual variables still gives an unique solution in terms of primal variables, i.e., the speeds. So, if one is interested only in trajectories of falling blocks, for example, this is not a problem. Neither it is a major problem for the iterative solver that we use to solve the CCP: iterations still converge to one of the many solutions for contact reactions.

However, although computable, multiple solutions for dual variables represents a problem because at each time step the CCP solver may converge to a different solution of $\widehat{\gamma}$ even if blocks show little or no motion. This triggers a noisy display of contact forces that seems to cycle between different solution sets, although with the same net result.

Moreover, such over-constrained problems are too sensitive to initial parameters. One can see PFCCQ as an extension of the Mangasarian-Fromoviz Constraint Qualification (MFCQ) - actually, for frictionless contacts, the two definitions coincide - and it is known that the MFCQ property is related to the Lipschitz stability of the solution with respect to perturbation parameters.

For the reasons above, we decided to introduce a regularization in form of a numerical compliance in contacts. This is similar to what presented in [39] for LCP problems; here regularization of the CCP is easily achieved by modifying the Delassus operator of (33), adding a diagonal part E, $e_{i,i} > 0 \; \forall i$, that is

$$N \;\; = \;\; D^T {M^{(l)}}^{-1} D + E \, . \tag{43}$$

By doing this, the N matrix (which was originally positive-semidefinite because of the high rank-deficiency of D), becomes a positive definite matrix with smallest eigenvalue at least as small as $\min(e_{i,i})$. Thanks to this regularization, we get the uniqueness of the solution for the dual variables, and the solver converges stably to the same solution at each timestep.

In [49] we showed that it is useful to make E block diagonal with $E_i = (h^2 K_i)^{-1}$, where $K_i \in \mathbb{R}^{3\times 3}$ is a diagonal matrix with the normal and tangential (u, v) stiffness of the i-th contact point. This done, we can exploit regularization to model a side effect: compliance in contacts.

One might argue that this introduction of compliance is a departure from the original idea of using perfectly rigid blocks, but we remark that this is still different from a penalty approach because it still fits in the variational formalism for non-smooth set-valued forces. Hence our time integration algorithm retains the good stability even when taking large time steps. Also, it is not necessary to use physical compliance values that match the stiffness of the real materials. An almost-rigid behaviour can be obtained by using extremely small non physical values; these will make N positive definite anyway and will provide uniqueness of $\boldsymbol{\gamma}$ solutions. *Vice versa*, one might want to increase compliance in sake of fast or even real-time simulations. In fact, our numerical tests showed that the higher the compliance parameter, the faster the convergence of the iterative solver.

3 Examples of architectural masonry structures under static loads

In order to show the potentiality of the proposed method, we now consider paradigmatic case studies mainly consisting in voussoir arches under static loading, whose failure modes are well studied and demonstrated by experience. Comparisons are made with the analysis based upon the most classical thrust-line graphical method, which provides a synthetic visualization of the path of compressive forces within the arch contours [42].

3.1 Typical failure modes in voussoir arches

Considering as possible planes of instability only the contact surfaces between the voussoirs, the *conventional* thrust-line graphical method consists in verifying the moment equilibrium. Since the problem is in general statically undetermined, several static states can be found for the arch under self-weight and applied loads, each of which can be synthetically described by a thrust line, obtained from vector addition as a funicular polygon. The thrust line tends to become a curve in the limit of voussoirs of infinitesimal thickness, with the property that the resultants of the contact forces between consecutive voussoirs are tangent to it. Under the assumptions that no sliding can occur between the blocks, a simple extension of plastic limit-analysis theorems assures that moment equilibrium is achieved if at least one thrust line can be found that completely lies within the section of the structure. Actually thought under the no-sliding hypothesis, the method is integrated with an *a posteriori* ascertain, which consists in verifying that the inclination of one admissible thrust line to the contact surface between the voussoirs is less than the friction angle.

Likewise the thrust line approach, also the NSCD method requires the knowledge of only the friction coefficient and density of the material. In order to visualize a pure moment failure, the first case study is that of a stand-alone arch under self weight and concentrated loads, as represented in Figure 6(a). The friction coefficient has been artificially made very high ($\mu = 0.8$), so to avoid sliding between the blocks. The NSCD model predicts the collapse mechanism of Figure 6(b) when the concentrated loads are in total of the order of 10% of the weight of the arch. This is in agreement with the finding from the conventional thrust-line graphical method, since this is the threshold beyond which no thrust line can remain within the section of the arch. Figure 6(a) represents the corresponding limit conventional thrust line; comparison with Figure 6(b) indicates that hinged rotations occur around those points where the thrust line touches the contours of the arch.

If one considers a more realistic value of the friction coefficient such as $\mu = 0.4$, the concentrated loads at failure are much lower than in the previous case, of the order of 6% of the weight of the arch. Figure 7(a) represents the limit thrust line, which touches the arch profile at the crown and at the haunches, but not at the springers. In agreement, the collapse mechanism predicted by the NSCD method (Figure 7(b)) represents the formation

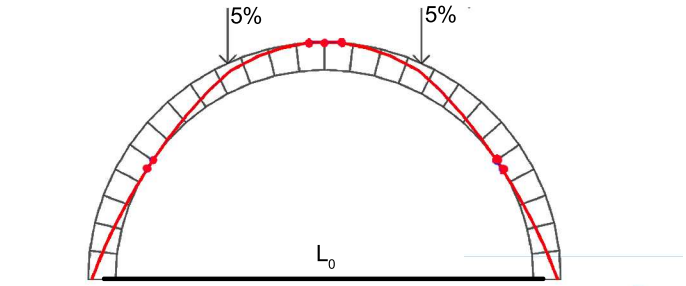

(a)

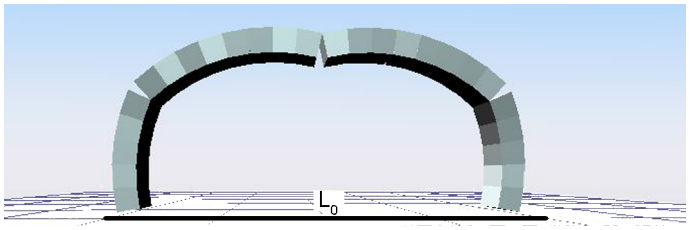

(b)

Figure 6: Stand-alone arch under self weight and concentrated forces (in percentage of self weight) with *high friction* coefficient ($\mu = 0.8$). a) Layout, bond pattern and conventional thrust line. b) Collapse mechanism predicted by the model.

of hinges at the crown and at the haunches. However, the low friction coefficient allows that the springers of the arch slide horizontally with respect to the imposts. An a posteriori analysis indicates that the inclination of the thrust at the springer voussoir interface is greater than the assumed friction angle for this case.

These numerical experiments reproduce the most well-known failure mechanism of voussoir arches, but the potentiality of the NSCD approach can be better appreciated when the bond pattern produces complex interactions between the blocks. In Figure 8 spandrels have been added to the same arch of Figure 7, with the only difference that the outer profile has been shaped so to accommodate the blocks forming the spandrels. Figure 8(a) represents the bond pattern with indication of the applied concentrated loads, again evaluated as a percentage of the weight of the sole arch. The conventional thrust line, here also illustrated, has been calculated by assuming that the arch structure is isolated and loaded by the spandrels weight, i.e., the interaction with the spandrel walls is neglected since they are simply considered as a dead weight on the arch. The failure load calculated with the thrust line method is of the order of 40% of the weight of the sole arch. This is confirmed by the NSCD simulations of Figure 8(b), which represent the collapse mechanism in a stand alone arch under such external concentrated loads and the dead weight of the blocks above.

Meanwhile, the numerical analysis of the whole block assembly, represented in Figure 8(d), indicates that no collapse mechanism occurs under the aforementioned loads. This is

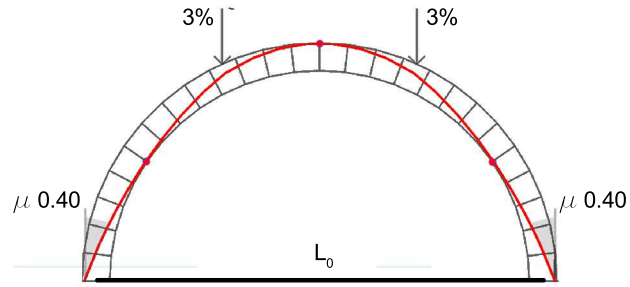

(a)

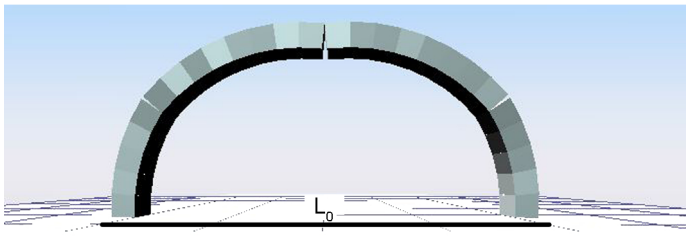

(b)

Figure 7: Stand-alone arch under self-weight and concentrated forces (in percentage of self weight) with friction coefficient $\mu = 0.4$. a) Layout and conventional thrust line. b) Collapse mechanism predicted by the model.

confirmed by the *effective* thrust line of Figure 8(c), which has been drawn by considering the envelope of the resultants of the actual forces transmitted through each contact plane between adjacent voussoirs, as calculated by the NSCD code. Remarkably, the shape of the conventional thrust line is quite different from the effective one. Whereas the first one is quite similar to a polygon, due to the high concentrated loads that are dominant with respect to the self-weight, the second one is much smoother and rounded and evidences the action of horizontal forces associated with the confinement effects produced by the spandrels.

In this case study, the conventional thrust line approach is conservative because no sliding between the blocks occurs, so that the hypotheses of the static theorem of limit analysis are a posteriori verified. However, the conventional method does not provide information about the safety level. In the real case, the critical load is higher than its prediction because not only the weight, but even more so the kinematic confinement of the spandrels stabilizes the arch. The discrepancy between the results from the conventional and the NSCD approaches increases as the geometry and the loading conditions become more complex. For example, if the concentrated loads were applied on the top of the surmounting wall, rather than on the outer profile of the arch, the thrust line method would provide the same results, but the collapse load would substantially increase, because of the spreading out of the load through the wall before reaching the arch.

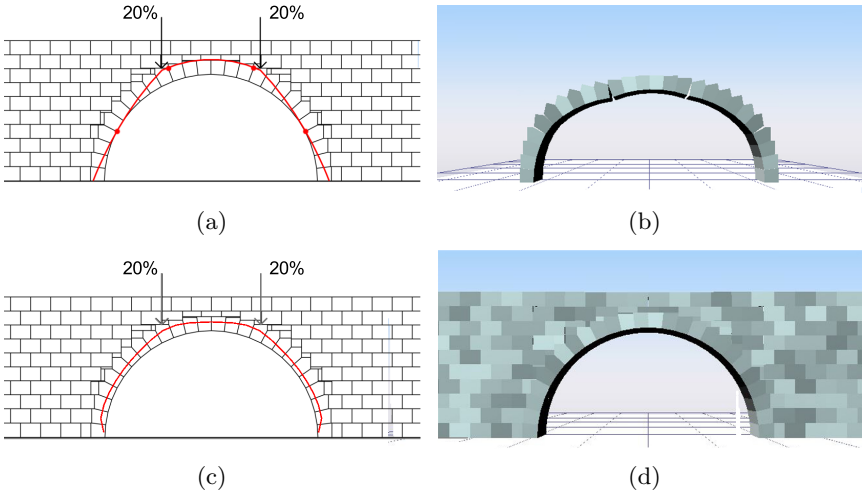

Figure 8: Spandrel arch with friction coefficient $\mu = 0.4$ under *moderate concentrated loads* (in percentage of the weight of the sole arch). a) Bond pattern and conventional thrust line. b) Collapse of the *equivalent* (stand alone) arch under the external and spandrel loads. c) Effective thrust line in the spandrel arch. d) Safe response from the NSCD model.

3.2 Flow of internal forces within masonry structures

From the comparison between the *conventional* and the *effective* thrust lines of Figure 8, it is evident that the path of forces within the arch is often incorrectly represented by the conventional method of analysis. In particular, it emerges that the loads directly supported by the arch are different from the dead weight of the surmounting wall. The reason for this discrepancy is that a natural arch may form in a wall with a regular bond pattern, which is able to directly support the blocks above it.

To better illustrate this important point, in Figure 9(a) we consider the case of a simple wall, with the same regular bond pattern of the previous spandrels, whose base is not supported in a central portion for a width equal to the span of the arch previously considered. As one may expect, a portion of the wall falls down under the action of the sole self-weight, as represented by the NSCD simulation of Figure 9(b). Figure 9(c) illustrates the resultants of the contact forces between the horizontal joints of the blocks (the length of the segment is proportional to the intensity of the forces). This confirms that there is an inactive triangular-shaped portion (the one that falls down), while the remaining part of the wall creates a natural arch, a triangular shaped structure strongly compressed especially at the springers, which can sustain the weight of the blocks above it. This behaviour was widely employed in ancient times through the construction of the so called *corbelled arches*, of which a particularly celebrated example from 1500 b.C. is the *Portico* of the tomb of Clytemnestra at Mycenae, represented in Figure 9(d).

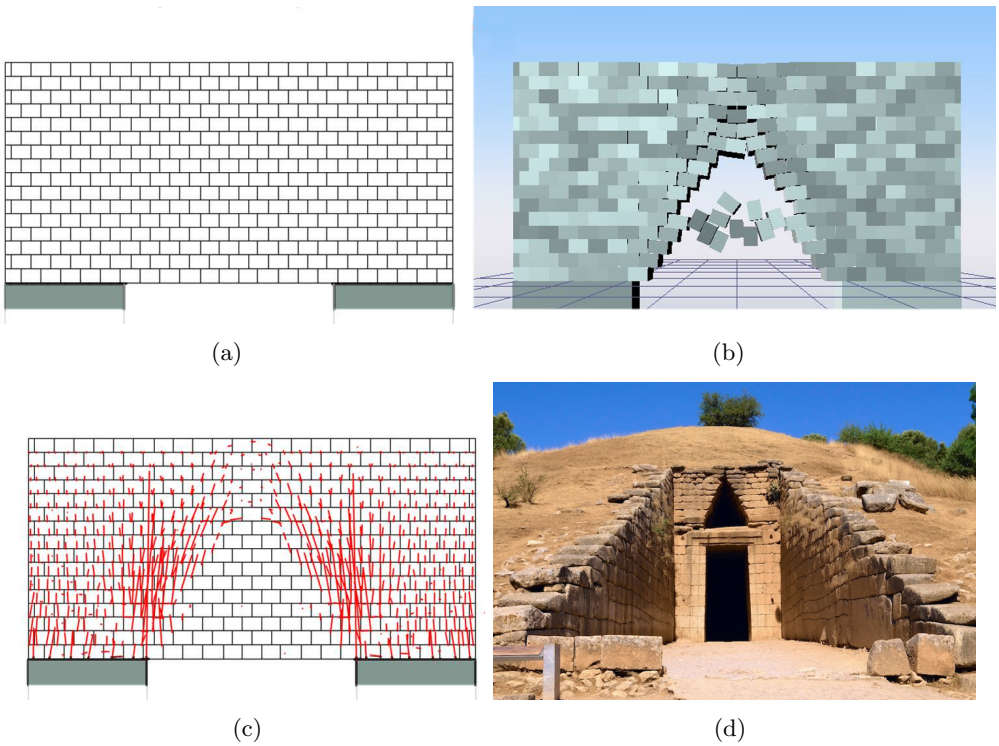

(a) (b)

(c) (d)

Figure 9: Natural arch formed in a wall ($\mu = 0.4$) under self-weight. a) Layout. b) Collapse mechanism from the NSCD model. c) Resultants of contact forces between horizontal joints. d) Corbelled arch in the *Portico* of the Tomb of Clytemnestra, Mycenae, c. 1500 b.C.

The corbelled arches consist of successive courses of masonry placed on both sides of the opening, and projecting inwards closer and closer. The same principle can be used in 3-D constructions, creating false dome shapes that were widely employed in ancient times. Such shapes can be considered the 3-D counterpart of the case study proposed in Figure 9.

Therefore, assume a cylindrical assembly of blocks, radially constructed, whose overall height and span are equal to the height and span of the wall analyzed before. The base of the cylinder is not supported in a central, octagonal area, whose circumscribed diameter is the same as the length of the unsupported portion in Figure 9(a). The results from the numerical simulations, with one quarter of the cylinder hidden for visual clarity, are represented in Figure 10(a) (bottom up view) and Figure 10(b) (lateral view). The natural formation of a false dome shape is evident. One may note how the central blocks are kept in place by the 3-D confining action of the other blocks. The 3-D flow of stress is verified by the representation of the contact forces on the horizontal joints, represented in Figure 10(c). The direction of the forces is from the central axis toward the supports, similarly to the 2-D case but not planar, of course. Figure 10(d) suggests again, as a paradigmatic example of corbelled dome, the Tomb of Clytemnestra in Mycenae, which is accessed from the *Portico* of Figure 9(d).

The examples just illustrated confirm that the proposed method of analysis presents a twofold advantage. First, it allows evaluating the failure mechanism of complex 2-D and 3-D masonry structures; second, by leveraging on the speed and robustness of the NSCD formulation, its work-flow allows interactive pre- and post-processing of the data, hence promoting a direct understanding of the results.

4 Dynamics

The NSCD approach is now applied to the transient simulation of a wall subjected to ground motion. This is a benchmark for evaluating the efficiency of the NSCD method in the context of dynamic problems involving masonry structures, as it happens in seismic analysis, explosions, controlled building demolition and so on.

The case considered is the same of Figure 8, already discussed for the static case. The wall is 5.0 m tall, 0.8 m thick, 16.2 m long, and contains an arch opening of radius 3.8 m. Blocks have density 1800 kg/m^3 and friction coefficient $\mu = 0.4$, while no additional forces, apart from the self weight, are active. A global orthogonal reference system is introduced such that x is the horizontal axis in the plane of the arch (parallel to the ground plane), y is the in-plane vertical axis, and z is the out-of-plane axis. A sinusoidal motion of the ground is applied, with a frequency of $f = 1$ Hz and an amplitude $A = 0.2g/(4\pi^2 f^2)$, where g denotes the gravity acceleration, so that the Peak Ground Acceleration (PGA) is $\sim 0.2g$. We discuss the structural response when the motion is acting, not simultaneously, into the two orthogonal horizontal x and z directions. We simulated the motion for 6 s and, in both

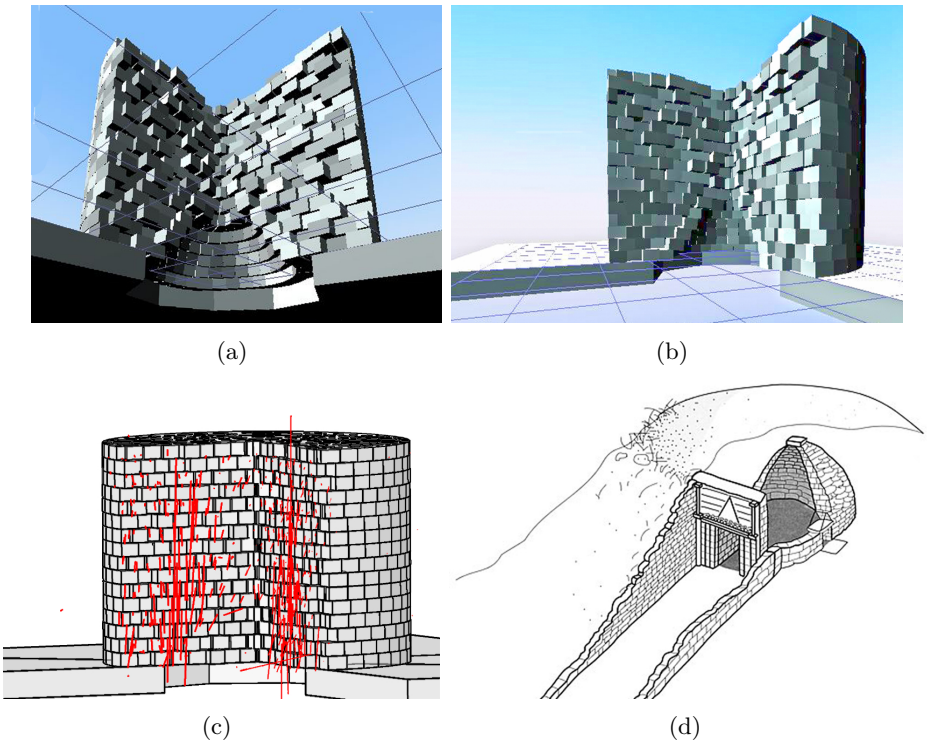

Figure 10: Domeshaped space formed in a partially supported masonry cylinder ($\mu = 0.4$) under self-weight. a) Surviving blocks after partial collapse (bottom up view) as predicted by the NSCD approach. b) Side view after partial collapse. c) Resultants of the contact forces between horizontal joints. d) Corbelled dome in the Tomb of Clytemnestra, Mycenae, c. 1500 b.C.

cases, this was sufficient to reach the arch collapse.

The time step used for the simulations is $h = 0.001$ s. We have experienced that shorter time steps do not change the results and, indeed, one can still obtain stable simulations (at the cost of lower precision) even with very large time steps, up to $h = 0.02$ s. For comparison, we performed similar simulations using conventional methods with ODE-DEM and penalty-based contacts, and we have verified that the simulation required at least three-orders-of-magnitude shorter time steps to avoid divergent results. This finding shows the advantages of the NSCD approach, which in fact can simulate the collapse almost in real-time using a commercial 2GHz Intel©i7 4510U quad-core processor.

Figure 11 represents the response to a ground motion in the longitudinal direction (x axis). Figure 11(a) shows sequential pictures of the moving structure, whereas Figure 11(b) records the plots, as a function of time, of the displacements of the ground "d_g", and of the keystone block "d_b" (marked with a white dot in Figure 11(a)); the latter is split into the three x, y and z components. Remarkably, the acceleration transmitted by the ground induces the collapse in a structure that is safe under the pure static action of its self weight. The motion of the keystone block is almost negligible in the $z-$direction, which is orthogonal to the ground acceleration. In the $x-$direction, the keystone block is affected by the ground motion, but the corresponding displacement, though presenting variable sign, does not exhibit the same frequency. This is probably due to the fact that the natural vibration frequencies of the wall, which do vary with time because they depend upon the degree of damage (disassembly) induced during the motion, are lower than the frequency of the ground acceleration.

As a matter of fact, what should be noticed is the monotonically increasing vertical displacement ($y-$component) of the keystone block. It is worth mentioning that we have also analyzed the static response of the structure when static body forces, equal to the block density multiplied by the GPA, are applied in the $x-$direction (equivalent static analysis) and added to the self weight, but this condition is safe according to the NSCD simulation. This means that an oscillating action can be more dangerous than a static one with the same peak. In fact, it is the shaking action due to the ground oscillation that is capable of inducing the local collisions of the blocks, which results in a motion that tends to provoke detachment of the contact surfaces, thus reducing the frictional forces and their stabilizing effect.

Figure 12 is the counterpart of Figure 11 when the ground motion is in the transversal $z-$direction. Figure 12(b) shows that both the $x-$ and $z-$direction displacements of the keystone block are not negligible. In particular, the z component, after a transient state, tends to follow the oscillations of the ground with a comparable frequency, a motion that should be associated with the rocking in the $x - z$ plane, appreciable in Figure 12(a).

Also in this case, we observe the increasing displacement of the keystone block in the vertical $y-$direction, a sign of increasing collapse. If one considers a static analysis with the

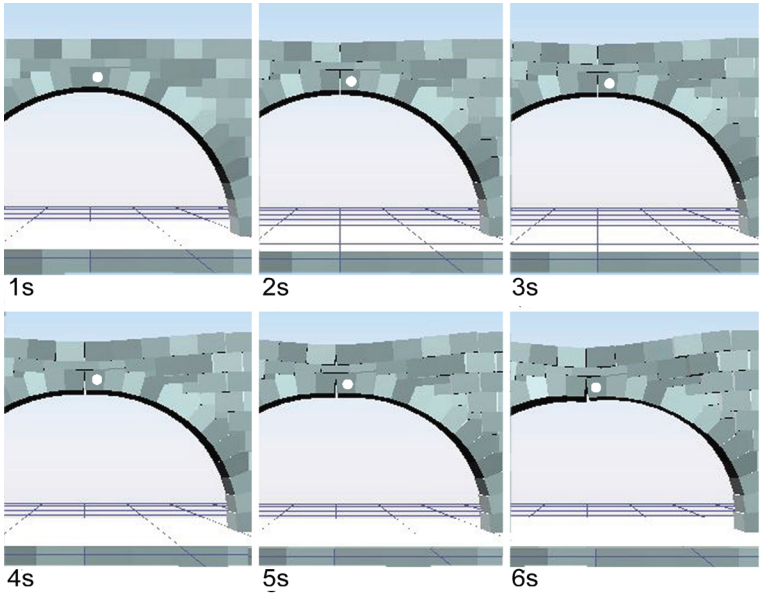

(a)

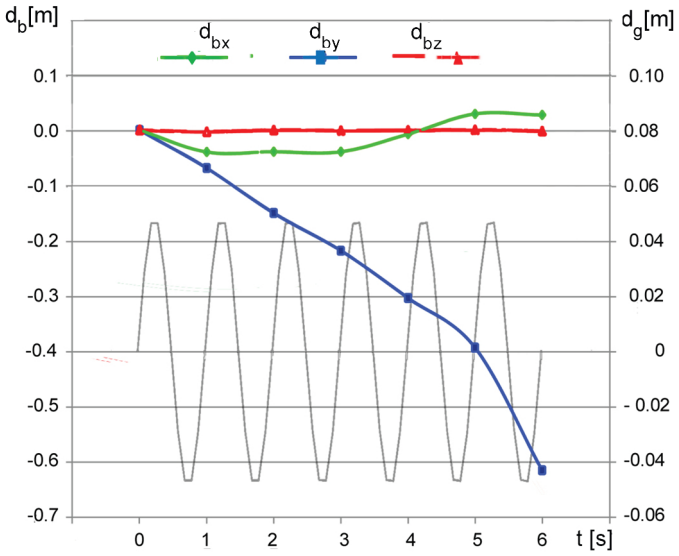

(b)

Figure 11: Spandrel arch under horizontal in-plane (x-direction) oscillatory ground displacement ($PGA \simeq 0.2$g and $f = 1$ Hz). a) Failure steps derived from the NSCD simulation. b) Comparison of the displacement of the ground (d_g) and of the keystone block (d_b), the latter in its three components (x = in-plane horizontal, y = in-plane vertical, z = out-of-plane horizontal).

same peak, one finds that there is no sliding of the blocks, because the frictional coefficient ($\mu = 0.4$) is again compatible with a PGA$\simeq 0.2g$ applied in horizontal direction. However, due to the small thickness of the arch in the $z-$direction, the whole assembly flips over at the base, as if it was a rigid block.

The examples just presented indicate that it is very important to analyze the local interactions and collisions of the blocks when studying dynamic motions, because possible detachments can provoke the reduction, or even the annihilation, of the frictional forces that provide the stabilizing contribution to the assembly. Since motions of this kind are associated with non-smooth velocities fields, the NSCD approach overtakes by far the performance achievable by ODE-DEM approaches and penalty-based contacts.

5 Discussion and Conclusions

A Non-Smooth Contact Dynamics (NSCD) model based upon a Differential Variational Inequality (DVI) and Cone Complementary Problem (CCP) formulation has been numerically implemented and applied to analyze constructions made by rigid blocks in frictional unilateral contact. Peculiarities of this approach are the procedure for contact detection and the consequent regularization, which guarantees uniqueness of solution with great benefits in terms of numerical performance. Being interested in a comprehensive approach, we have integrated the NSCD simulator, developed within the Project Chrono platform, with parametric design tools that allow elaborating complex source geometries and post-processing the results from the analyses. It is thus possible to graphically express in real time the resultant of the contact forces between any two blocks and sum them up, for example to visualize the effective thrust line in arched structures. Although the constitutive input is simply represented by density and friction angle, the model can interpret the response of masonry-like structures under static and dynamic loading.

In order to describe the potentialities of the model, paradigmatic structures have been tested. Where applicable, we have made comparisons with the classical graphical thrust line method to assess the stability of masonry structures, proving that it may provide misleading results essentially due to the effects of friction. Meanwhile, the more common Ordinary Differential Equation (ODE) approach with penalty-based contacts, as implemented in Discrete Element Method (DEM) software, is difficult to be applied given the high number of parameters. Since in the NSCD formulation the velocity field may be highly irregular, the proposed approach can accurately detect the interaction and collisions between the constituent blocks as a consequence of imposed ground accelerations, as in the case of an earthquake. Since this local motion can provoke the local detachment of the blocks, thus reducing or even annihilating the frictional forces that stabilize the assembly, structures can fail even if they result safe under equivalent static loading, i.e., under the peak ground acceleration supposed constantly applied in time. With respect to ODE-DEM methods, the efficiency of the NSCD approach can be better appreciated under dynamic forcing, and the

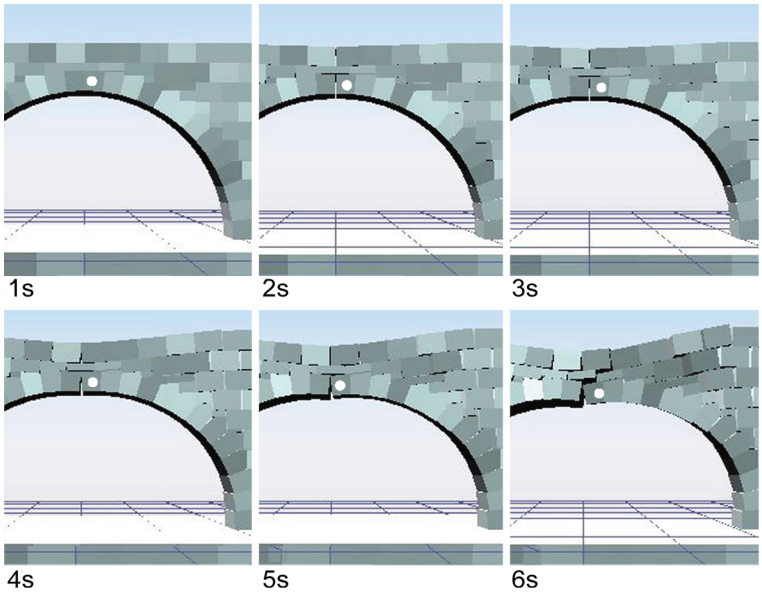

(a)

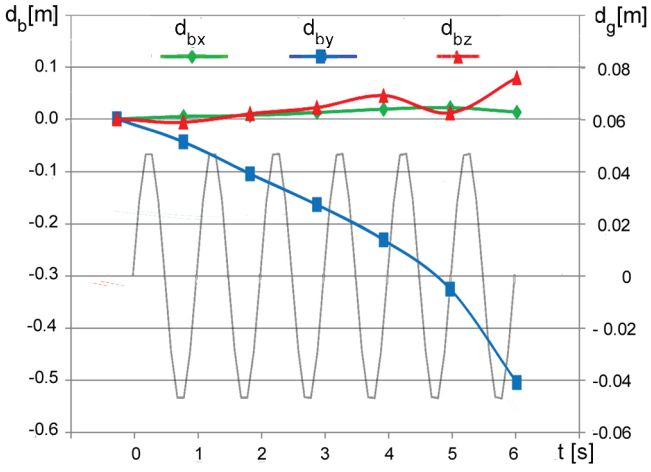

(b)

Figure 12: Spandrel arch under horizontal out-of-plane (z-direction) ground displacement ($PGA \simeq 0.2$g and $f = 1$ Hz). a) Failure steps derived from the NSDC simulation. b) Comparison of the displacement of the ground (d_g) and of the keystone block (d_b), the latter in its three components (x = in-plane horizontal, y = in-plane vertical, z = out-of-plane horizontal).

method of solution is very efficient even when applied to structures composed by a great number of blocks. The smooth match of the two working environment (Project Chrono platform and parametric design tool) is yet to be fully appreciated. Further developments will consist in the analyses of vaults, domes and other classical masonry structures.

Acknowledgements. The authors are grateful to Raffaello Bartelletti (Bartelletti Design Bureau, Pisa, Italy) for inspiring discussion during the preparation of this work. G.R.C. acknowledges the partial support of the Italian *Ministero dell'Istruzione, dell'Università e della Ricerca* under grant MIUR-PRIN voce COAN 5.50.16.01 code 2015JW9NJT.

References

[1] Vincent Acary and Bernard Brogliato. *Numerical methods for nonsmooth dynamical systems: applications in mechanics and electronics*, volume 35. Lect. N. App. Comput. Mech. 35 Springer Verlag, 2008.

[2] Mihai Anitescu. Optimization-based simulation of nonsmooth rigid multibody dynamics. *Math. Program.*, 105(1):113–143, 2006.

[3] Mihai Anitescu and Gary D. Hart. A constraint-stabilized time-stepping approach for rigid multibody dynamics with joints, contact and friction. *International Journal for Numerical Methods in Engineering*, 60(14):2335–2371, 2004.

[4] Mihai Anitescu and Gary D. Hart. A fixed-point iteration approach for multibody dynamics with contact and friction. *Mathematical Programming, Series B*, 101(1)(ANL/MCS-P985-0802):3–32, 2004.

[5] Mihai Anitescu and Alessandro Tasora. An iterative approach for cone complementarity problems for nonsmooth dynamics. *Computational Optimization and Applications*, 47(2):207–235, 2010.

[6] D. Bigoni and G. Noselli. Localized stress percolation through dry masonry walls. part i - experiments. *European Journal of Mechanics, A/Solids*, 29(3):291–298, 2010.

[7] D. Bigoni and G. Noselli. Localized stress percolation through dry masonry walls. part ii - modelling. *European Journal of Mechanics, A/Solids*, 29(3):299–307, 2010.

[8] Ernesto G. Birgin, Jos Mario Martnez, and Marcos Raydan. Nonmonotone spectral projected gradient methods on convex sets. *SIAM Journal on Optimization*, 10(4):1196–1211, 2000.

[9] C. Casapulla and F. Portioli. Experimental and analytical investigation on the frictional contact behavior of 3d masonry block assemblages. *Construction and Building Materials*, 78:126–143, 2015.

[10] P. Clemente, A. Occhiuzzi, and A. Raithel. Limit behavior of stone arch bridges. *Journal of Structural Engineering (United States)*, 121(7):1045–1050, 1995.

[11] Erwin Coumans. http://bulletphysics.org, 2012.

[12] P. A. Cundall and O. D. L. Strack. A discrete numerical model for granular assemblies. *Geotechnique*, 29(1):47–65, 1979.

[13] C. de Coulomb. Essay sur une application des règles de maximis et minimis à quelques problèmes de statique, relatif à l'architecture. *Mémoires de mathmatique & de physique, présentés à l'Académie Royale des Sciences par divers savans*, 7:343–382, 1776.

[14] Daniel Charles Drucker. Coulomb friction, plasticity and limit loads. *Journal of Applied Mechanics*, 21(1):71–74, 1954.

[15] F. Dubois and M. Jean. *The non-smooth contact dynamic method: recent LMGC90 software developments and application*, pages 375–378. Springer Berlin Heidelberg, Berlin, Heidelberg, 2006.

[16] S.S. Keerthi E.G. Gilbert, D.W. Johnson. A fast procedure for computing the distance between complex objects in three-dimensional space. *Robotics and Automation*, 4(2):193–203, 1988.

[17] R. Fosdick and G. Royer-Carfagni. The constraint of local injectivity in linear elasticity theory. *Proceedings of the Royal Society A: Mathematical, Physical and Engineering Sciences*, 457(2013):2167–2187, 2001.

[18] M. François and G. Royer-Carfagni. Structured deformation of damaged continua with cohesive-frictional sliding rough fractures. *European Journal of Mechanics, A/Solids*, 24(4):644–660, 2005.

[19] M. Gilbert. Limit analysis applied to masonry arch bridges: state-of-the-art and recent developments. In *Proceedings 5th International Conference on Arch Bridges*, pages 13–28, Madeira, 2007.

[20] M. Gilbert, C. Casapulla, and H.M. Ahmed. Limit analysis of masonry block structures with non-associative frictional joints using linear programming. *Computers and Structures*, 84(13-14):873–887, 2006.

[21] M. Gilbert and C. Melbourne. Rigid block analysis of masonry structures. *Structural engineer London*, 72(21):356–361, 1994.

[22] E. Hairer and G. Wanner. *Solving Ordinary Differential Equations*, volume II of *Computational Mathematics*. Springer-Verlag, 1991.

[23] J. Heyman. Equilibrium of masonry arches. *Proceedings of the Institution of Civil Engineers. Engineering and Computational Mechanics*, 163:129–133, 2010.

[24] Toby Heyn, Mihai Anitescu, Alessandro Tasora, and Dan Negrut. Using krylov subspace and spectral methods for solving complementarity problems in many-body contact dynamics simulation. *International Journal for Numerical Methods in Engineering*, 95(7):541–561, 2013.

[25] Michel Jean. The non-smooth contact dynamics method. *Computer Methods in Applied Mechanics and Engineering*, (177):235–257, 1999.

[26] David Kinderleher and Guido Stampacchia. *An Introduction to Variational Inequalities and Their Application*. Academic Press, New York, 1980.

[27] A. Kooharian. Limit analysis of voussoirs (segmental) and concrete arches. *Proceedings American Concrete Institute*, 49:317, 1953.

[28] G. Lancioni, D. Gentilucci, E. Quagliarini, and S. Lenci. Seismic vulnerability of ancient stone arches by using a numerical model based on the non-smooth contact dynamics method. *Engineering Structures*, 119:110–121, 2016.

[29] Giovanni Lancioni, Stefano Lenci, Quintilio Piattoni, and Enrico Quagliarini. Dynamics and failure mechanisms of ancient masonry churches subjected to seismic actions by using the {NSCD} method: The case of the medieval church of s. maria in portuno. *Engineering Structures*, 56:1527 – 1546, 2013.

[30] R.K. Livesley. Limit analysis of structures formed from rigid blocks. *International Journal for Numerical Methods in Engineering*, 12(12):1853–1871, 1978.

[31] H. Mazhar, T. Heyn, A. Pazouki, D. Melanz, A. Seidl, A. Bartholomew, A. Tasora, and D. Negrut. Chrono: a parallel multi-physics library for rigid-body, flexible-body, and fluid dynamics. *Mechanical Sciences*, 4(1):49–64, 2013.

[32] J. J. Moreau. *Unilateral Contact and Dry Friction in Finite Freedom Dynamics*, pages 1–82. Springer Vienna, Vienna, 1988.

[33] Jean J. Moreau and Michel Jean. Numerical treatment of contact and friction: The contact dynamics method. In *Proceedings of the Third Biennial Joint Conference on Engineering Systems and Analysis*, page to appear, Montpellier, France, July 1996.

[34] J.J. Moreau. Numerical aspects of the sweeping process. *Computer Methods in Applied Mechanics and Engineering*, 177(3-4):329 – 349, 1999.

[35] Agustn Ordua and Paulo B. Loureno. Cap model for limit analysis and strengthening of masonry structures. *Journal of Structural Engineering*, 129(10):1367–1375, 2003.

[36] P. Painlevé. Sur le lois du frottement de glissemment. *Comptes Rendus Acad. Sci. Paris*, 121:112–115, 1895.

[37] Jong-Shi Pang and David Stewart. Solution dependence on initial conditions in differential variational inequalities. *Mathematical Programming*, 116:429–460, 2009.

[38] Jong-Shi Pang and David E. Stewart. Differential variational inequalities. *Mathematical Programming*, 113(2):345–424, 2008.

[39] Constantin Popa, Tobias Preclik, and Ulrich Rüde. Regularized solution of lcp problems with application to rigid body dynamics. *Numerical Algorithms*, 69(1):145–156, 2015.

[40] Xiuzhi Qu and Brent Stucker. A 3d surface offset method for stl-format models. *Rapid Prototyping Journal*, 9(3):133–141, 2003.

[41] Ali Rafiee, Marc Vinches, and Claude Bohatier. Application of the {NSCD} method to analyse the dynamic behaviour of stone arched structures. *International Journal of Solids and Structures*, 45(2526):6269 – 6283, 2008.

[42] Pere Roca, Miguel Cervera, Giuseppe Gariup, and Luca Pela'. Structural analysis of masonry historical constructions. classical and advanced approaches. *Archives of Computational Methods in Engineering*, 17(3):299–325, 2010.

[43] G. De Saxc and Z.-Q. Feng. Recent advances in contact mechanics the bipotential method: A constructive approach to design the complete contact law with friction and improved numerical algorithms. *Mathematical and Computer Modelling*, 28(4):225 – 245, 1998.

[44] David E. Stewart. Convergence of a time-stepping scheme for rigid body dynamics and resolution of Painleve's problems. *Archive Rational Mechanics and Analysis*, 145(3):215–260, 1998.

[45] David E. Stewart. Rigid-body dynamics with friction and impact. *SIAM Review*, 42(1):3–39, 2000.

[46] David E. Stewart. Reformulations of measure differential inclusions and their closed graph property. *Journal of Differential Equations*, 175:108–129, 2001.

[47] David E. Stewart and Jeffrey C. Trinkle. An implicit time-stepping scheme for rigid-body dynamics with inelastic collisions and Coulomb friction. *International Journal for Numerical Methods in Engineering*, 39:2673–2691, 1996.

[48] D.E. Stewart. Existence of solutions to rigid body dynamics and the Painlevé paradoxes. *C. R. Acad. Sci. Paris*, 325:689–693, 1997.

[49] A. Tasora, M. Anitescu, S. Negrini, and D. Negrut. A compliant visco-plastic particle contact model based on differential variational inequalities. *International Journal of Non-Linear Mechanics*, 53(0):2 – 12, 2013. Multibody System Dynamics: A Selective Perspective.

[50] G.P.A.G. van Zijl. Modeling masonry shear-compression: Role of dilatancy highlighted. *Journal of Engineering Mechanics*, 130(11):1289–1296, 2004.